Transgenic mouse models in migraine

Ven, R.C.G. van de

THREE

CHAPTER 3

Gene dosage-dependent transmitter release changes at neuromuscular synapses of *Cacna1a* R192Q knockin mice are non-progressive and do not lead to morphological changes or muscle weakness

S. Kaja[1,2], R.C.G. van de Ven[3], L.A.M. Broos[3], H. Veldman[4], J.G. van Dijk[1], J.J.G.M. Verschuuren[1], R.R. Frants[3], M.D. Ferrari[1], A.M.J.M. van den Maagdenberg[1,3] and J.J. Plomp[1,2]

[1]Department of Neurology and Clinical Neurophysiology, [2]Department of Neurophysiology, [3]Department of Human Genetics, Leiden University Medical Centre, Leiden, The Netherlands

[4]Rudolf Magnus Institute of Neuroscience, Department of Neurology and Neurosurgery, Section Neuromuscular Diseases, University Medical Centre Utrecht, Utrecht, The Netherlands

Neuroscience 135 (2005) p. 81–95

Abstract

$Ca_v2.1$ channels mediate neurotransmitter release at the neuromuscular junction (NMJ) and at many central synapses. Mutations in the encoding gene, *CACNA1A*, are thus likely to affect neurotransmitter release. Previously, we generated mice carrying the R192Q mutation, associated with human familial hemiplegic migraine type-1, and showed first evidence of enhanced presynaptic Ca^{2+} influx.[1] Here, we characterize transmitter release in detail at mouse R192Q NMJs, including possible gene-dosage dependency, progression of changes with age, and associated morphological damage and muscle weakness. We found, at low Ca^{2+}, decreased paired-pulse facilitation of evoked ACh release, elevated release probability, and increased size of the readily releasable transmitter vesicle pool. Spontaneous release was increased over a broad range of Ca^{2+} concentrations (0.2-5 mM). Upon high-rate nerve stimulation we observed some extra rundown of transmitter release. However, no clinical evidence of transmission block or muscle weakness was found, assessed with electromyography, grip-strength testing and muscle contraction experiments. We studied both adult (~3-6 months-old) and aged (~21-26 months-old) R192Q knockin mice to assess effects of chronic elevation of presynaptic Ca^{2+} influx, but found no additional or progressive alterations. No changes in NMJ size or relevant ultrastructural parameters were found, at either age. Our characterizations strengthen the hypothesis of increased Ca^{2+} flux through R192Q-mutated presynaptic $Ca_v2.1$ channels and show that the resulting altered neurotransmitter release is not associated with morphological changes at the NMJ or muscle weakness, not even in the longer term.

Abbreviations

ACh, acetylcholine; BTx, α-bungarotoxin; CMAP, compound muscle action potential; CNS, central nervous system; CSD, cortical spreading depression; EA2, episodic ataxia type-2; EPP, endplate potential; FHM, familial hemiplegic migraine; KI, knockin; MEPP, miniature endplate potential; NMJ, neuromuscular junction; PBS, phosphate-buffered saline, RNS-EMG, repetitive nerve stimulation electromyography

Introduction

Neuronal $Ca_v2.1$ (P/Q-type) Ca^{2+} channels are expressed widely in the central nervous system (CNS), where they mediate neurotransmitter secretion.[2] In the mammalian peripheral nervous system, expression of $Ca_v2.1$ channels is mainly restricted to the neuromuscular junction (NMJ), where P-type channels regulate acetylcholine (ACh) release.[3] The pore-forming subunit of the $Ca_v2.1$ channel is encoded by the *CACNA1A* gene[4,5], and P- and Q-type channels are splice variants of this gene possessing different sensitivities to the neurotoxins ω-agatoxin-IVA and ω-conotoxin-MVIIC.[5,6] Mutations in *CACNA1A* have been identified in familial hemiplegic migraine type-1 (FHM1), episodic ataxia type-2 (EA2), spinocerebellar ataxia type-6 and forms of epilepsy.[7-10] Furthermore, natural mouse mutants exist with epilepsy and ataxia (for reviews, see [11,12]).

In view of the importance of $Ca_v2.1$ channels in neurotransmitter release, we may expect that *CACNA1A* mutations result in either increased or decreased release. This may cause synaptic dysfunction in the CNS, contributing to neurological symptoms. Besides, dysfunction may be present at NMJs and might, for instance, share features with Lambert-Eaton myasthenic syndrome, where auto-antibodies target presynaptic $Ca_v2.1$ channels, resulting in reduced transmitter release.[13] Impaired NMJ transmission seems present in EA2 patients with *CACNA1A* mutations[14,15], and has been suggested in patients with common types of migraine without mutations.[16,17] No abnormalities have been found in SCA-6 [18,19] nor in FHM1 with the I1811L mutation.[20]

We recently generated a knockin (KI) mouse, carrying the human FHM1 R192Q mutation [1]. These mice showed a decreased trigger threshold for cortical spreading depression (CSD, the mechanism underlying the migraine aura) and increased cellular Ca^{2+} influx due to a shift in the activation voltage of $Ca_v2.1$ channels. At the NMJ we demonstrated profound increase in spontaneous uniquantal ACh release and increase of action potential-evoked release, at low-rate stimulation in the presence of low extracellular Ca^{2+} concentration. These findings indicated increased presynaptic Ca^{2+} influx.

Here we performed a more detailed *ex vivo* electrophysiological characterization of transmitter release in R192Q KI mice, as well as a morphological analysis of NMJs. By studying both homo- and heterozygous R192Q KI mice we assessed a possible gene-dosage dependency, of relevance because FHM1 is an autosomal dominant disorder. Since functional NMJ defects may lead to muscle weakness, we assessed neuromuscular transmission with *in vivo* repetitive nerve stimulation electromyography (RNS-EMG) and muscle strength measurements, and with *ex vivo* muscle contraction experiments. Chronically elevated presynaptic Ca^{2+} influx may cause damage and eventually lead to synaptic apoptosis.[21] Therefore, we also studied NMJ function of aged (21-26 months-old) R192Q KI mice.

Material and Methods

Mice

Generation of the R192Q KI mouse strain has been described previously.[1] In short, codon 192 in exon 4 of the mouse *Cacna1a* gene was modified by mutagenesis now encoding a glutamine instead of an arginine residue. By gene targeting approach, agouti offspring was obtained carrying the transgene. For the experiments, transgenic mice were used in which the neomycin-resistance cassette was deleted using mice of the EIIA-Cre deleter strain that express Cre recombinase driven by the EIIA early promoter.[22] Heterozygous mice (96% C57BL/6J background) were subsequently interbred to provide litters containing all three possible genotypes that were used for the experiments. Male and female mice were used in different age groups (~3 - 26 months), as specified in the Results. Litters were genotyped after weaning, as described previously.[1] All experiments were carried out with the investigator blinded for genotype, and confirmatory genotyping was done after the experiment.

All experiments were carried out according to Dutch law and Leiden University guidelines, and were approved by the Leiden University Animal Experiments Commission.

Ex vivo electrophysiological recordings at the NMJ

Mice were killed by carbon dioxide inhalation. Phrenic nerve-hemidiaphragms were dissected and mounted in standard Ringer's medium (in mM: NaCl 116, KCl 4.5, $CaCl_2$ 2, $MgSO_4$ 1, NaH_2PO_4 1, $NaHCO_3$ 23, glucose 11, pH 7.4) at room temperature. The medium was continuously bubbled with 95% O_2 / 5% CO_2. In some experiments soleus and flexor digitorum muscles of the right hind leg were dissected as well. Intracellular recordings of miniature endplate potentials (MEPPs), the spontaneous depolarizing events due to uniquantal ACh release and endplate potentials (EPPs, the depolarisation resulting from nerve action potential-evoked ACh release) were made at NMJs at 28 °C using standard micro-electrode equipment, as described previously.[23] At least 30 MEPPs and EPPs were recorded at each NMJ, and at least 10 NMJs were sampled per experimental condition per mouse. Muscle action potentials, mediated by Na^+ channels, were blocked by 3 μM of the selective muscle Na^+ channel blocker μ-conotoxin GIIIB (Scientific Marketing Associates, Barnet, Herts, UK). In order to record EPPs, the phrenic nerve (or tibial nerve, in case of soleus muscle) was stimulated supramaximally at 0.3 Hz and 40 Hz. The amplitudes of EPPs and MEPPs were normalized to –75 mV, assuming 0 mV as the reversal potential for ACh-induced current[24], using the following formula:

$EPP_{normalized} = EPP \times (-75/V_m)$, where V_m is the measured resting membrane potential. The normalized EPP amplitudes were corrected for non-linear summation with an *f* value of 0.8.[25] Quantal content, i.e. the number of ACh quanta released per nerve impulse, was calculated by dividing the normalized and corrected mean EPP amplitude by the normalized mean MEPP amplitude.

Release parameters *n* (releasable vesicle pool) and *p* (release probability) were calculated from EPP and MEPP data using the method of Miyamoto, based on binomial statistics.[26] MEPPs were also recorded shortly after exposure of preparations to hypertonic medium (0.5 M sucrose Ringer), as alternative assessment of the pool of ACh vesicles ready for immediate release.[27]

In some experiments the effect of 200 nM of the selective $Ca_v2.1$ channel blocker ω-agatoxin-IVA or of 2.5 μM of the $Ca_v2.2$ blocker ω-conotoxin-GVIA (both toxins from Scientific Marketing Associates) was tested on ACh release, following a 20 min pre-incubation period.

Electron microscopy and ultrastructural quantification

Diaphragm preparations were pinned out and fixed in 2% paraformaldehyde, 2% glutaraldehyde (both Sigma, Zwijndrecht, The Netherlands) in 0.1 M phosphate buffered saline pH 7.4 (PBS) for one hour at 4 °C. Endplate regions were excised and cut in small blocks. After washing overnight with PBS, blocks were postfixed in 1% osmium tetroxide in phosphate buffer for 2 hours. The tissue was then dehydrated in a graded series of acetone and embedded in epoxy resin (Serva, Heidelberg, Germany).[28]

Semi-thin sections (1 μm) were stained with toluidine blue and used to identify the NMJ containing region of the muscle. Ultra-thin sections (60-80 nm) were cut with an LKB Ultrotome III and mounted on coated copper grids. Sections were contrasted with uranyl acetate and Reynold's lead citrate[29] and viewed under a JEOL 1200 EX electron microscope (Jeol, Peabody, MA).

Electron micrographs were analysed using Sigma Plot Pro v4.0 (Jandel Scientific, San Rafael, CA). Measurements were performed with the investigator blinded for genotype. We used strict inclusion criteria: a synaptic profile was defined as a structure exhibiting parallel pre- and postsynaptic membranes with a discernable synaptic cleft bordered by Schwann cells, a postsynaptic density, and dense amounts of clear vesicles at the presynaptic terminal. Nerve terminal profiles were quantified by conducting measurements and counts for: (1) area of the nerve terminal, (2) perimeter of the nerve terminal, (3) synaptic length, defined as the length of the presynaptic membrane between the capping Schwann cell profiles, (4) area of postsynaptic junctional folds, and (5) number of vesicles in randomly placed 200 x 200 nm boxes in the region adjacent to the

presynaptic membrane. Furthermore, the muscle contact ratio (synaptic length expressed as proportion of the perimeter) was determined, quantifying the degree of retraction of the nerve terminal from the muscle surface. The postsynaptic index (synaptic length expressed as proportion of postsynaptic junctional fold area) provides an indication of size and complexity of postsynaptic folds.

α-Bungarotoxin staining and image analysis

NMJ size was determined by staining the area of ACh receptors with fluorescently labelled α-bungarotoxin (BTx), which irreversibly binds to ACh receptors. Diaphragm preparations were pinned out and fixed in 1% paraformaldehyde (Sigma, Zwijndrecht, The Netherlands) in 0.1 M phosphate-buffered saline (PBS), pH 7.4, for 30 minutes at room temperature. Following a 30 minute wash in PBS, diaphragms were incubated in 1 μg/ml Alexa Fluor 488 conjugated BTx (Molecular Probes, Leiden, The Netherlands) in PBS for 3 hours at RT. After a final washing step in PBS (30 minutes), endplate regions were excised and mounted on microscope slides with Citifluor AF-1 antifadent (Citifluor, London, UK). Sections were viewed using an Axioplan microscope (Zeiss, Jena, Germany). NMJs were identified on the basis of BTx staining, under standardized camera conditions. Images of BTx stain were stored on hard disk; quantification was carried out in Scion Image (Scion Corporation, Frederick, Maryland). In total, four diaphragms per genotype were quantified. In every diaphragm, ten NMJs were selected based upon randomly generated coordinates. Length, width and perimeter of the BTx-stained area were measured.

Ex vivo muscle contraction experiments

Left phrenic nerve-hemidiaphragm preparations were mounted in a dish containing 10 ml Ringer medium. The central tendon was connected via a hook and a string to a K30 force transducer (Harvard Apparatus, March-Hugstetten, Germany). The signal was amplified by a TAM-A bridge-amplifier (Harvard Apparatus) and digitized by a Digidata 1200B digitizer (Axon Instruments, Union City, USA), connected to a personal computer running Axoclamp 9.0 data-acquisition software (Axon Instruments). The nerve was placed on a bipolar stimulation electrode. Supramaximal stimuli (usually ~10 V) of 100 μs duration were delivered every 10 min for 3 s at 40 Hz from a Master-8 programmable stimulator (AMPI, Jerusalem, Israel). Basic tension was adjusted with a vernier control to obtain maximal stimulated tetanic contraction force (usually about 10 g). Medium was continuously bubbled with 95% O_2 / 5% CO_2. Stability of the elicited contraction was monitored for one hour. Thereafter the medium was replaced every hour

with 10 ml Ringer medium containing increasing concentration (250, 500, 750, 1000 and 1500 nM) of d-tubocurarine (Sigma-Aldrich, Zwijndrecht, The Netherlands). Amplitude of contractions was cursor-measured in Clampfit 9.0 (Axon Instruments), 2 s after start of the each nerve stimulation train. At the end of each experiment, d-tubocurarine was washed out to observe complete recovery of the initial contraction force.

Grip strength assessment

Muscle strength was measured using a grip strength meter for mice (600 g range; Technical and Scientific Equipment GmbH, Bad Homburg, Germany), connected to a laptop computer. The test was carried out essentially as originally described for rats.[30] The peak force of each trial was considered the grip strength. Each mouse performed five trials, each about 30 s apart. The mean value of the five trials was used for statistical analysis.

Repetitive nerve stimulation electromyography (RNS-EMG)

Wild-type and R192Q KI mice (24 months of age) were anaesthetized with a 15:1 (v/v) mixture of ketamine hydrochloride (Ketalar®; 10 mg/ml, Parke-Davis, Hoofddorp, The Netherlands) and medetomidine hydrochloride (Domitor®; 1 mg/ml, Pfizer, Capelle a/d IJssel, The Netherlands), at 8 µl per g body weight administered intraperitoneally.

Subcutaneous recording needles were inserted in the plantar aspect of the hind foot, and needle-stimulating electrodes were inserted near the sciatic nerve in the thigh. Using a portable Nicolet Viking Quest (Nicolet Biomedical, Madison, WI), responses from foot muscles were recorded following supramaximal stimulation (150% of the stimulus intensity giving a maximal response). Trains of 10 stimuli were applied at 0.2, 1, 3, and 5 Hz, with a 2-minute recovery period between each train.

Data were analysed in a custom-written Matlab (The MathWorks Ics., Natick, MA) analysis routine, performing base-line correction as well as spline interpolation. Compound muscle action potential (CMAP) amplitude and area of the initial negative peak were measured for all CMAPs in a train, and the largest decrease ('decrement') of amplitude or area during the train was identified and expressed as percentage of the value of the first CMAP in a train.

Statistical analyses

In the *ex vivo* electrophysiological and fluorescence microscopical analyses we measured 5-15 NMJs per muscle per experimental condition. The mean muscle value was calculated from the mean values of the parameters obtains at individual NMJs and was subsequently used to calculate group mean values with n as the number of mice. In the electronmicroscopical analyses we calculated the genotype mean from the values obtained from n= ~20 nerve terminal profiles, originating from four mice per genotype. In the grip-strength measurements, electromyography and *ex vivo* muscle contraction experiments n is the number of mice measured. The data is given as mean ± S.E.M., unless indicated otherwise. Possible statistical differences were analysed with a paired or unpaired Student's *t*-test, analysis of variance (ANOVA) with Tukey's HSD post-hoc test, or non-parametric Mann-Whitney test where appropriate. In all cases a *p*-value of <0.05 was considered to be statistically significant.

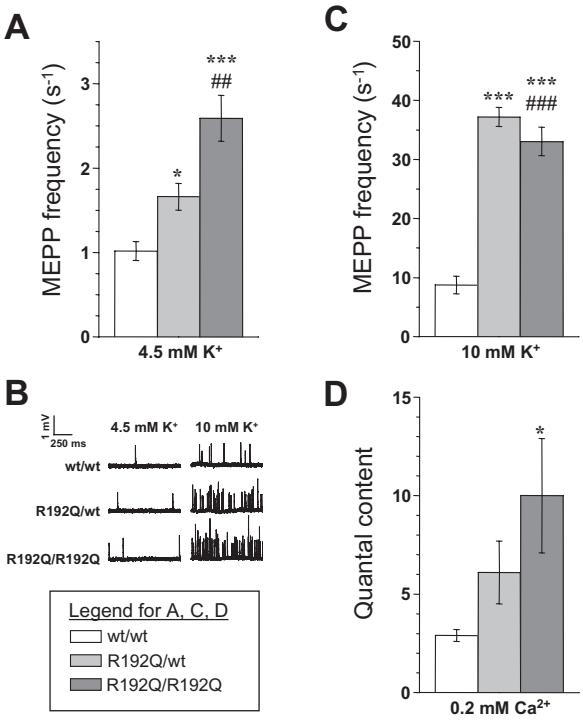

Figure 1. R192Q gene dosage dependent increase of ACh release at diaphragm NMJs. (**A**) MEPP frequency of R192Q heterozygous (n=6) mice lies in between values obtained at wild-type (n=7) and homozygous (n=5) mice, measured in normal (4.5 mM) K^+. (**B**) Typical examples of MEPP recordings (1 s traces). (**C**) MEPP frequency under depolarizing conditions (10 mM K^+ Ringer's medium). The increase of mean MEPP frequency was pronounced at homo- and heterozygous R192Q NMJs (14- and 23-fold, respectively), compared with wild-type (8-fold), as tested for with ANOVA (n=5-16, $p<0.001$), leading to equally high MEPP frequency at hetero- and homozygous R192Q NMJs. (**D**) Quantal content at low (0.2 mM) extracellular Ca^{2+} is increased at R192Q-mutated synapses (ANOVA $p<0.05$). The increases are 110% at heterozygous ($p=0.36$) and 240% at homozygous ($p<0.05$) R192Q-mutated NMJs. *$p<0.05$, **/## $p<0.01$, ***/### $p<0.001$, where asterisks indicate a difference from wild-type and hashes from heterozygote. Data represented as grand means ± S.E.M of n muscles; 10-15 NMJs tested per muscle.

Results

The increase in ACh release at R192Q NMJs is gene-dosage dependent

Previously we showed ~2-fold increase in spontaneous ACh release and ~3-fold increase in low-rate nerve-stimulation evoked release (at 0.2 mM Ca^{2+}) at NMJs of homozygous R192Q KI mice.[1] We investigated the dependence of these effects on the amount of R192Q-mutated alleles, in view of the dominant inheritance pattern of human FHM1. Release parameters at diaphragm NMJs of 3 months-old heterozygous R192Q mice were studied with *ex vivo* electrophysiology. MEPP frequency was intermediate between that observed at wild-type and homozygous R192Q NMJs (1.66 ± 0.16, 1.02 ± 0.11 and 2.59 ± 0.27 s^{-1}, respectively; n=5-7, Fig. 1A, B). The selective $Ca_v2.1$ blocker ω-agatoxin-IVA (200 nM) reduced MEPP frequency at heterozygous R192Q NMJs to 0.53 ± 0.07 s^{-1} (n=4), a level similar to that found after toxin treatment of wild-type and homozygous R192Q NMJs.[1] Slight depolarization of heterozygous R192Q NMJs by incubation with 10 mM K^+-Ringer induced an increase of MEPP frequency to a level that was equal to that observed in homozygous R192Q NMJs (37.18 ± 1.62 /s, i.e. ~400% of the wild-type value, n=4-16, Fig. 1B, C). Low-rate (0.3 Hz) evoked ACh release at 0.2 mM Ca^{2+} at heterozygous R192Q NMJs was also intermediate between wild-type and homozygote (6.1 ± 1.6, 2.9 ± 0.3, and 10.0 ± 2.9, respectively; n=5-7, Fig. 1D). These results show a gene-dosage effect of the R192Q mutation on spontaneous ACh release and low-rate evoked release (at 0.2 mM Ca^{2+}), and a dominant effect on release induced by 10 mM K^+.

Altered rundown of high-rate evoked ACh release at R192Q NMJs

Some effects of the R192Q mutation on transmitter release may only become apparent at high intensity use of the $Ca_v2.1$ channel. Therefore, we measured ACh release at high-rate (40 Hz) nerve stimulation. During a stimulation period of 1 s, the observed EPP amplitude rundown at homozygous diaphragm R192Q NMJs of 3 months-old mice was more pronounced only during the first 20 stimuli (Fig. 2, $p<0.05$). EPP rundown at heterozygous R192Q NMJs was intermediate between homozygous R192Q and wild-type rundown profile during this initial phase of the stimulus train, again indicating gene-dosage dependency. After the 20th stimulus these extra EPP rundowns recovered, however, to a similar plateau level as observed at wild-type NMJs (82.3 ± 0.6, 82.2 ± 1.7 and 84.0 ± 0.7% of the first EPP amplitude at wild-type, heterozygous and homozygous R192Q NMJs, respectively;n=6-8, $p=0.325$).

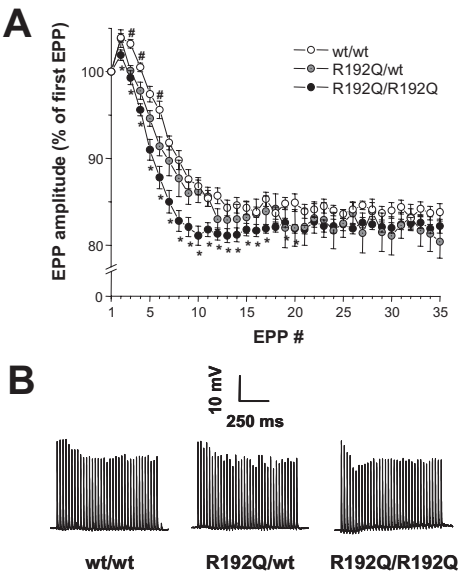

Figure 2. Increased rundown of ACh release at high-rate (40 Hz) stimulation. (**A**) EPP amplitudes across all genotypes ran down to similar plateau levels at about 82% of the first EPP in the trains (ANOVA, n=6-8, p=0.325). However, at R192Q NMJs a somewhat more pronounced initial rundown of EPP amplitudes was observed during the first 20 stimuli. Heterozygous R192Q synapses show an intermediate rundown profile in this phase.
* homozygous R192Q different from wild-type, p<0.05, # heterozygous R192Q different from wild-type, p<0.05. (**B**) Typical examples of EPP rundown profiles at 40 Hz stimulation.

Increase in spontaneous ACh release at R192Q NMJs in different muscle types

NMJs on different types of muscle fibres (i.e. slow- or fast-twitch) differ in structure and function.[31] Therefore, effects of R192Q mutation on transmitter release may differ in nature and/or extent among NMJs of different muscles. We measured ACh release electrophysiologically at NMJs of soleus (slow-twitch) and the flexor digitorum brevis (fast-twitch) muscle preparations of adult, 4.5 months-old R192Q KI mice. Increases in spontaneous ACh release, relative to wild-type, were observed (88%, p<0.01, in soleus and 133%, p<0.001, in flexor digitorum brevis, both n=4 muscles, Fig. 3A, B), comparable to those observed previously at NMJs of R192Q diaphragm[1], which contains a heterogeneous population of low- and fast-twitch fibres. As shown previously in diaphragm, 10 mM K^+ increased spontaneous ACh release disproportionally at R192Q NMJs, compared with wild-type, in soleus and flexor digitorum brevis muscle (Fig. 3A, B). Evoked (0.3 and 40 Hz) ACh release was measured at R192Q soleus NMJs in normal Ringer medium. Release at 0.3 Hz at R192Q NMJs in 2 mM Ca^{2+} was similar to wild-type (70.5 ± 2.0 and 74.0 ± 3.5, respectively, n=4, p=0.41, Fig. 3C), as in R192Q diaphragm. Rundown of ACh release at R192Q soleus NMJs during 40 Hz high-rate stimulation tended to be a little more pronounced than in wild-types (Fig. 3D), as observed at R192Q diaphragm NMJs (see above).

Ca^{2+}-dependency of transmitter release at R192Q synapses

$Ca_V2.1$ channels play a crucial role in controlling neurotransmitter release at many synapses, and there is a steep relationship between presynaptic Ca^{2+} influx and transmitter release. Hence, small changes in amplitude or time course of Ca^{2+} influx at the release sites can effectively modulate transmitter output when Ca^{2+} sensors are not saturated

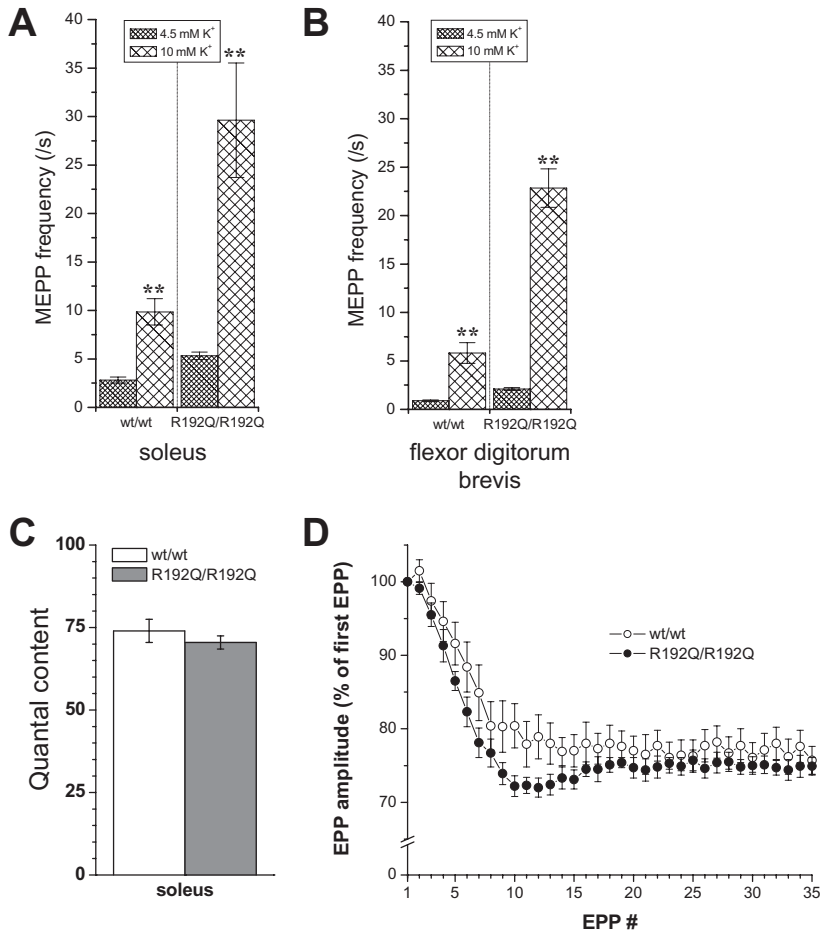

Figure 3. Electrophysiological changes at R192Q soleus and flexor digitorum brevis muscle NMJs. (**A**) The ~90% increase in MEPP frequency at R192Q soleus NMJs (n=4, $p<0.01$), compared to wild-type, rose to ~200% increase at 10 mM K^+ depolarization. (**B**). The ~130% increase in MEPP frequency at R192Q flexor digitorum brevis NMJs (n=4, $p<0.01$), compared to wild-type, rose to ~300% increase at 10 mM K^+ depolarization. (**C**) Quantal content at low rate (0.3 Hz) stimulation in the presence of physiological Ca^{2+} concentration (2 mM) did not differ between soleus R192Q and wild-type NMJs. (**D**) The rundown of EPP amplitude during 40 Hz nerve stimulation was somewhat (but not statistically significantly) more pronounced in the beginning phase of the trains. These observations are all similar to those observed at R192Q diaphragm NMJs. ** $p<0.01$.

during an action potential.[32] We previously reported that, in 0.2 mM Ca^{2+} medium, the quantal content at low rate (0.3 Hz) stimulation is ~340% of that of wild-type[1]. Here, we extended our Ca^{2+}-dependency experiments by studying spontaneous and low-and high-rate nerve stimulation-evoked ACh release at wild-type and homozygous R192Q NMJs from 3 months-old mice in a range of Ca^{2+} concentrations (0.01, 0.1, 0.2, 1, 2, and 5 mM). MEPP frequency at both R192Q and wild-type NMJs was greatly dependent on the Ca^{2+} concentration in the medium (Fig. 4A), with similar low values of ~0.1 s^{-1} at 0.01 and 0.1 mM Ca^{2+}. However, at higher Ca^{2+} concentrations, MEPP frequency at R192Q NMJs was consistently higher than at wild-types. Evoked release (0.3 Hz) differed only at 0.2 mM Ca^{2+} (Fig. 4B). Both at lower and higher concentrations tested, similar values were found, showing that Ca^{2+} concentrations around 0.2 mM are critical. This was also the case for high-rate evoked ACh release. Only at 0.2 mM Ca^{2+} the mean level of the

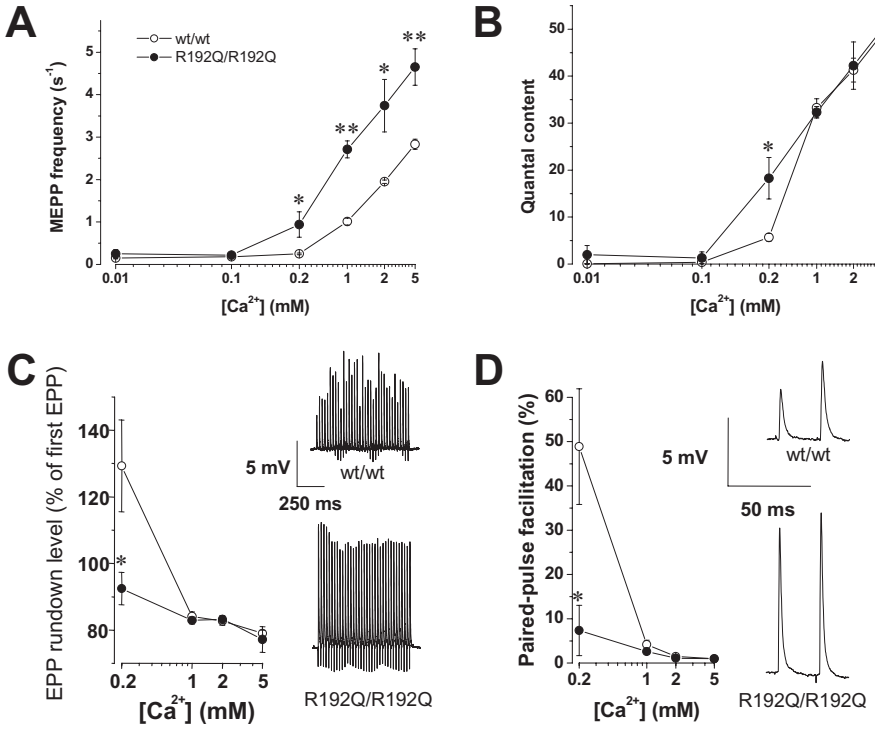

Figure 4. Ca^{2+}-dependency of ACh release parameters at R192Q NMJs. (**A**) Spontaneous ACh release. MEPP frequencies at NMJs of homozygous R192Q and wild-type mice were measured at 0.01 mM Ca^{2+} (n=4 mice, p=0.280), 0.1 mM Ca2+ (n=4, p=0.492), 0.2 mM Ca^{2+} (n=8, p<0.05), 1 mM Ca^{2+} (n=4, p<0.001), 2 mM Ca^{2+} (n=4, p<0.05) and 5 mM Ca2+ (n=4, p<0.01). (**B**) Evoked ACh release at 0.3 Hz nerve stimulation. Quantal contents were similar between genotypes at all tested Ca^{2+} concentrations, except at 0.2 mM Ca^{2+}, where quantal content was ~320% of that of controls (n=8, p<0.05), in accordance with our previous experimental series[1]. (**C**) EPP rundown level (mean amplitude of 21st-35th EPP, as percentage of the amplitude of the first EPP in the 40 Hz train) was ~93% at R192Q NMJs at 0.2 mM extracellular Ca^{2+}. Wild-type EPPs show ~30% run-up at this Ca^{2+} concentration. (**D**) Paired-pulse (25 ms interval) facilitation is more pronounced at wild-type NMJs in the presence of 0.2 mM Ca^{2+}. * p<0.05, ** P<0.01.

21st to 35th EPP in a 40 Hz train (expressed as percentage of the first EPP in the train) differed between R192Q and wild-type NMJs (93 ± 5% and 129 ± 14%, respectively, n=4, $p<0.05$, Fig. 4C). At all other Ca^{2+} concentrations tested (1, 2, 5 mM), rundown level averaged around 77-84% at both R192Q and wild-type NMJs. We looked at the first two pulses of 40 Hz trains at 0.2 mM Ca^{2+} to determine the amount of 25 ms paired pulse facilitation. This phenomenon of short-term synaptic facilitation appeared much larger at wild-type NMJs (49 ± 13%) than at R192Q NMJs (7 ± 6%, n=7, $p<0.05$, Fig. 4D).

We tested whether compensatory contribution of $Ca_v2.2$ (N-type) channels might be involved in the increase of spontaneous and evoked ACh release at 0.2 mM Ca^{2+} at R192Q NMJs. Application of the selective blocker ω-conotoxin-GVIA neither reduced MEPP frequency (0.42 ± 0.04 and 0.42 ± 0.06 s^{-1}, before and during toxin, respectively, n=3, $p=0.97$) nor 0.3 Hz quantal content (12.4 ± 3.1 and 12.6 ± 1.8, before and during toxin, respectively, n=3, $p=0.92$). Subsequent addition of $Ca_v2.1$ blocker ω-agatoxin-IVA reduced MEPP frequency to 0.23 (0.02 s-1 (n=3, $p<0.05$), and almost completely inhibited the quantal content, to 0.03 (0.01 (n=3, $p<0.05$). This indicates that R192Q mutant channels are solely responsible for the increase in ACh release at R192Q NMJs.

Increased release probability and vesicle pool at R192Q NMJs

Increased transmitter release is either caused by an increase in release probability (*p*) of synaptic vesicles, or an increase in the pool (n) of readily releasable vesicles[27]. Increased basal presynaptic Ca^{2+} influx through R192Q-mutated channels could in principle increase both *p*, by influencing the release machinery, and *n*, by stimulating second messenger pathways. We calculated both *p* and *n* from our EPP data obtained from diaphragm R192Q NMJs at various Ca^{2+} concentrations. At 0.2 mM, but not at higher extracellular Ca^{2+}concentration tested, *p* was much higher at R192Q than wild-type NMJs (0.69 ± 0.07 and 0.31 ± 0.20, respectively, n=6-7, $p<0.05$, Fig. 5A). Similarly, *n* was elevated (26.7 ± 6.4 and 7.1 ± 1.9, respectively, $p<0.01$, Fig. 5B). This was confirmed in alternative experiments to probe the vesicle pool size (MEPP frequency measurement in hypertonic, 0.5 M sucrose-Ringer): increased size at 0.2 mM Ca^{2+} (MEPP frequency 41.5 ± 4.1 and 61.5 ± 6.4 /s at wild-type and R192Q NMJs, respectively, n=4, $p<0.05$, Fig. 5C) and unchanged size at 2 mM Ca^{2+} (MEPP frequency 53.4 ± 10.3 and 50.4 ± 13.3 /s at wild-type and R192Q NMJs, n=5, $p=0.86$). These data indicate that the increased ACh release at 0.2 mM Ca^{2+} concentration follows from a combined effect of increased Ca^{2+} flux through R192Q-mutated channels on the release machinery and on the size of the readily releasable vesicle pool.

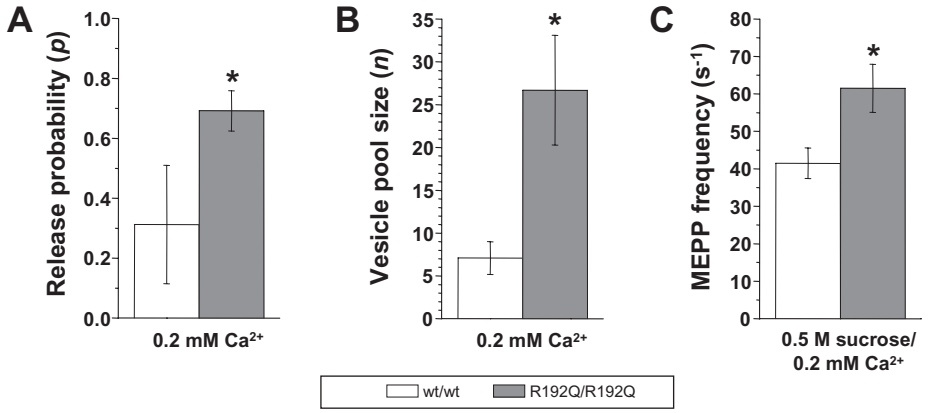

Figure 5. Increased release probability and readily releasable vesicle pool size at R192Q NMJs in Ringer's medium containing 0.2 mM Ca^{2+}. (**A**) The calculated ACh release probability p was 120% higher at R192Q NMJs (n=6, $p<0.05$). (**B**) The calculated size n of the pool of readily releasable vesicles was 276% higher at R192Q NMJs (n=6-7, $p<0.05$). (**C**) The pool of readily releasable vesicles, as assessed by measuring the MEPP frequency upon incubation of hypertonic medium (0.5 M sucrose Ringer), was 48% higher at R192Q NMJs (n=4, $p<0.05$). * $p<0.05$.

Morphology of R192Q neuromuscular synapses

The changes in ACh release parameters at R192Q NMJs could be caused by morphological changes, instead of resulting directly from the $Ca_v2.1$ mutation. For instance, increased MEPP frequency can result from synapse growth.[33,34] Therefore, we performed morphological analyses on NMJs of adult, 3-6 months-old mice. The size of NMJs, as estimated from staining with fluorescently labelled BTx, did not differ between genotypes (Fig. 6A-C). Detailed electron microscopical quantification of individual nerve terminals of homozygous R192Q KI mice, did not identify any ultrastructural abnormalities (Fig. 6D, E; Table 1).

Figure 6. Morphological features of R192Q NMJs. Fluorescently labelled α-bungarotoxin staining of (**A**) wild-type and (**B**) homozygous R192Q NMJs (scale bar: 15 μm). (**C**) Quantified parameters (perimeter, length, and width) did not differ between genotypes (p=0.197, P=0.192, and p=0.175, respectively). Grand means were obtained from four R192Q and four wild-type muscles, with ten NMJs quantified per genotype, and compared using Student's t-test. Electron microscopical micrographs of a single terminal profile of wild-type (**D**) and R192Q (**E**) muscle (scale bar: 1 μm). Quantification of morphological parameters of individual terminal boutons (n=17-22) did not reveal any ultrastructural abnormalities at R192Q NMJs (also see Table 1).

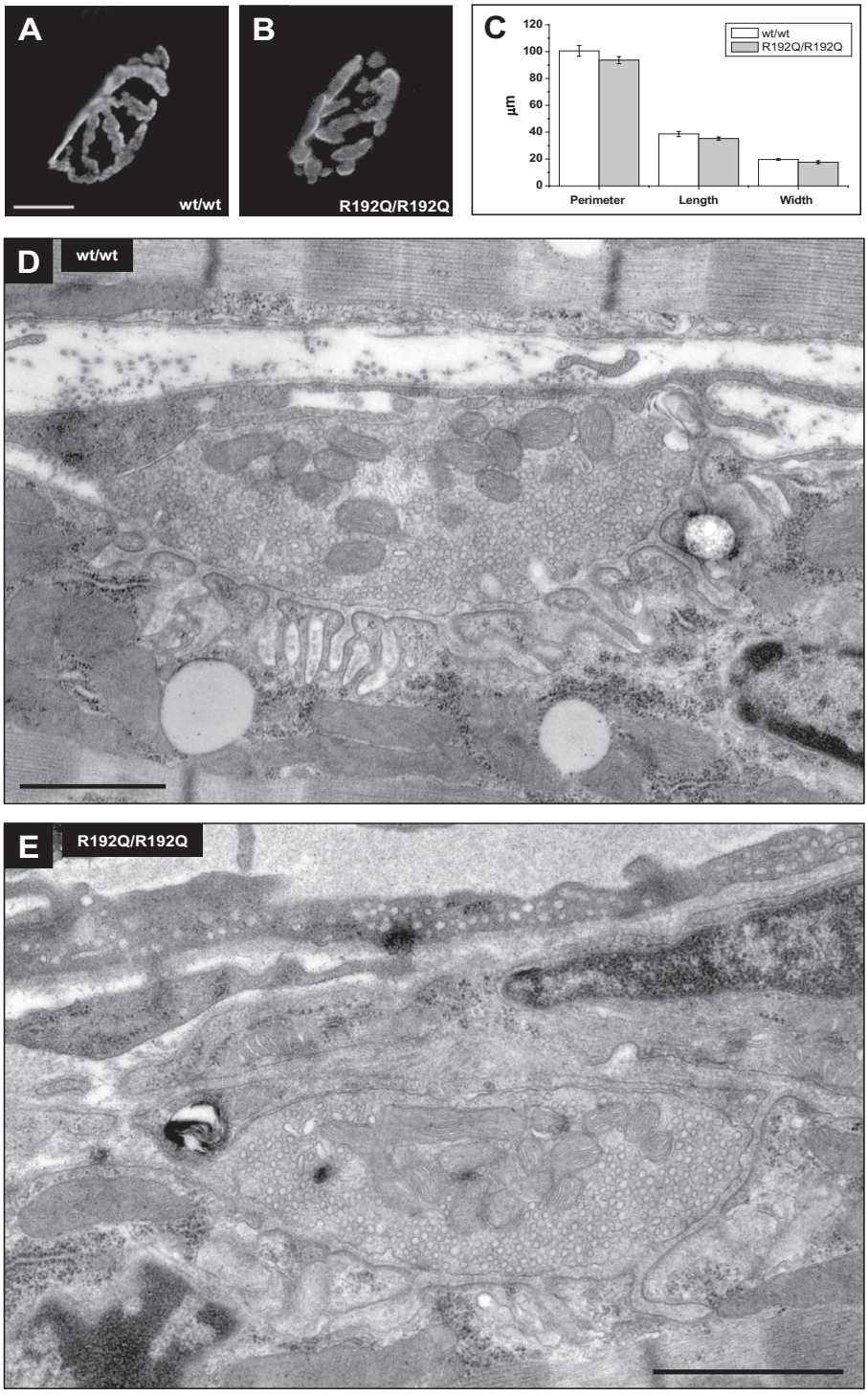
A
wt/wt
B
R192Q/R192Q
C
wt/wt
R192Q/R192Q
µm
120
100
80
60
40
20
0
Perimeter
Length
Width
D
wt/wt
E
R192Q/R192Q

Table 1. Ultrastructural parameters of R192Q nerve terminals

	Wild-type	R192Q	*P*
n (Diaphragms)/*n* (terminals)	4/22	4/17	
Number of terminal profiles per NMJ section	2.9±0.6	2.7±0.5	0.755
Nerve terminal area (μm^2)	5.15±0.99	4.35±1.25	0.279
Nerve terminal perimeter (μm)	12.66±1.76	12.42±2.65	0.566
Synaptic length (μm)	6.64±0.95	6.26±1.10	0.747
Area of postsynaptic folds (μm^2)	2.65±0.45	2.43±0.54	0.475
Muscle contact ratio	0.53±0.02	0.54±0.03	0.878
Postsynaptic index	0.49±0.04	0.42±0.06	0.255
Number of synaptic vesicles (per 200×200 nm)	9.69±0.22	9.21±0.18	0.138

Quantification of ultrastructural parameters was performed on pictures from 22 wild-type and 17 homozygous R192Q nerve terminal profiles, originating from diaphragms of four different 6 months-old mice per group. Values are the mean ± S.E.M. of the number of terminal profiles analysed. None of the quantified parameters differed between genotypes.

Assessment of ex- and in vivo neuromuscular transmission

Altered ACh release at NMJs may prevent successful synaptic transmission and, thus, cause muscle weakness. As described above, rundown of ACh release at high-rate nerve stimulation at diaphragm and soleus NMJs was more pronounced at 3-4.5 month-old R192Q KI mice. However, in *ex vivo* diaphragm muscle contraction experiments we did not observe increased d-tubocurarine sensitivity of R192Q muscles (Fig. 7A). Furthermore, we did not detect any differences between wild-type and R192Q KI animals (p=0.997) with *in vivo* grip-strength testing. The mean pulling forces were 90.2 ± 5.1 and 91.1 ± 6.3 g for wild-type and R192Q KI animals, respectively (n=15; Fig. 7B).

No progression of neuromuscular changes in aged (21-26 month-old) R192Q KI mice

We considered the possibility that increased presynaptic Ca^{2+} influx at R192Q NMJs may lead to long-term changes or damage. *Ex vivo* electrophysiological measurements were done at diaphragm NMJs of aged, 26 month-old R192Q KI mice. Increased MEPP frequency and a somewhat pronounced EPP rundown at 40 Hz stimulation were found, compared to wild-types (Fig. 8A, B). Furthermore, R192Q MEPP frequency increased disproportionally upon 10 mM K^+ depolarization (Fig. 8C). Also, low-rate (0.3 Hz) evoked ACh release remained similar at R192Q and wild-type NMJs of aged mice (Fig. 8D). The magnitudes of electrophysiological changes, compared with wild-type,

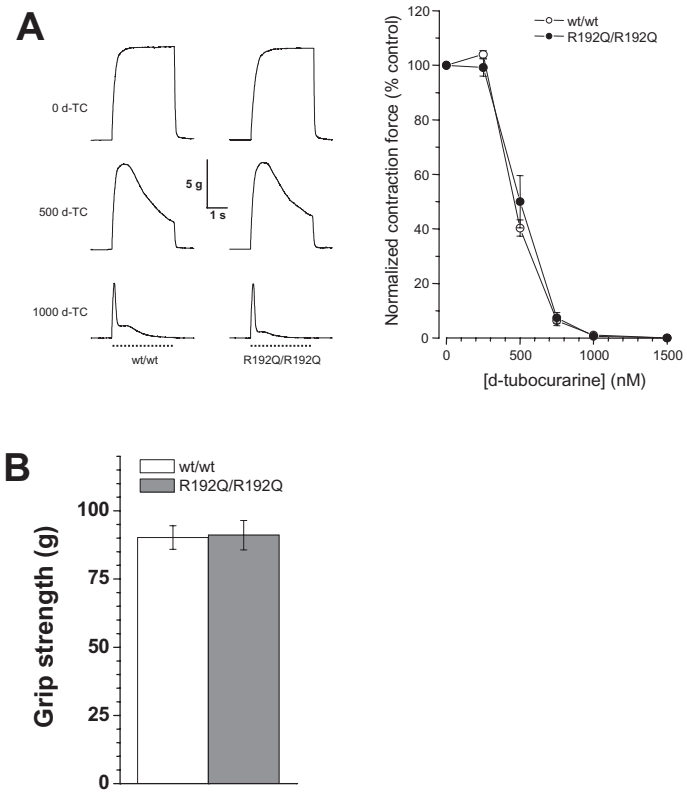

Figure 7. *In* and *ex vivo* assessment of neuromuscular function in 3-4.5 months-old R192Q KI mice. (**A**) Sensitivity of nerve stimulation evoked ex vivo muscle contraction to d-tubocurarine (d-TC) was equal for wild-type and R192Q diaphragm (n=4 and 5, respectively). Left-hand side of the panel shows typical contraction profiles upon 3 s supramaximal nerve stimulation after equilibration with 0, 0.5 and 1 µM d-tubocurarine in Ringer solution. Dotted lines indicate period of nerve stimulation. (**B**). R192Q KI mice did not show in vivo muscle weakness when assessing grip strength. The mean peak pulling force was about 90 g for both genotypes (Student's t-test, n=14-15, p=0.904).

observed at aged R192Q KI mice did not differ statistically significantly from that at young R192Q KI mice (Fig. 8E). The selective $Ca_v2.1$ blocker ω-agatoxin-IVA (200 nM) reduced MEPP frequency and quantal content at wild-type and R192Q NMJs (Fig. 8F) by a similar extent as reported before for young adult mice.[1] Thus, aberrant R192Q NMJ electrophysiology did neither progress nor change with age.

We also assessed *in vivo* neuromuscular function at aged R192Q KI mice. *In vivo* grip-strength testing revealed no differences in pulling force between 21 month-old R192Q KI and wild-type mice (Fig. 8G). Repetitive nerve-stimulation electromyography (RNS-EMG) was performed on anaesthetized 22 months-old wild-type and R192Q KI mice. The first CMAP amplitude in a train determined at a stimulation frequency of 0.2 Hz was 9.7 ± 2.7 mV and 9.8 ± 2.4 mV for wild-type and R192Q KI mice, respectively (n=4, p=0.978). With stimulus frequencies increasing up to 5 Hz, CMAP amplitudes

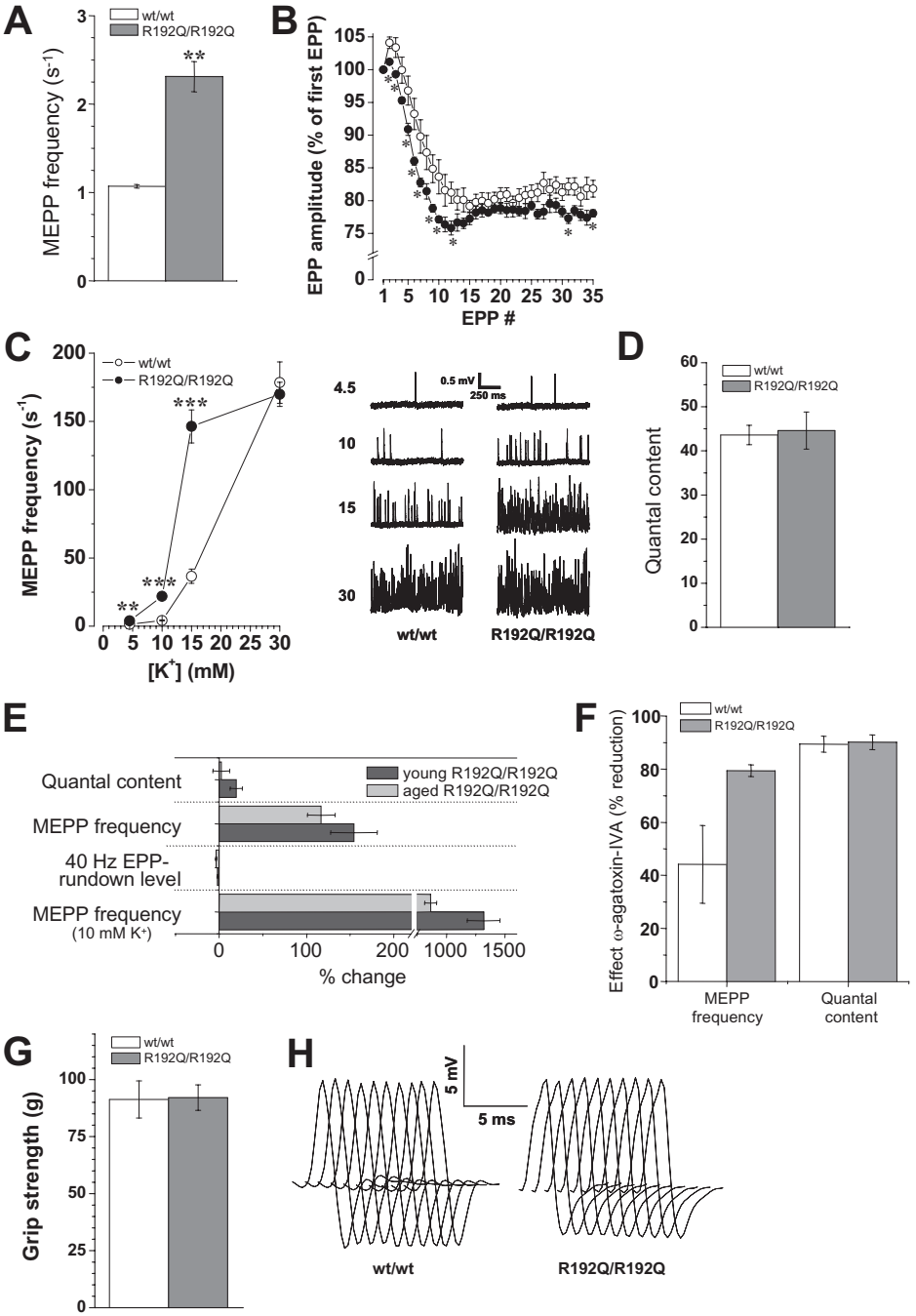
A
wt/wt
R192Q/R192Q
MEPP frequency (s-1)
B
EPP amplitude (% of first EPP)
EPP #
C
MEPP frequency (s-1)
[K+] (mM)
0.5 mV
250 ms
wt/wt
R192Q/R192Q
D
Quantal content
E
Quantal content
MEPP frequency
40 Hz EPP-rundown level
MEPP frequency (10 mM K+)
young R192Q/R192Q
aged R192Q/R192Q
% change
F
Effect ω-agatoxin-IVA (% reduction)
MEPP frequency
Quantal content
G
Grip strength (g)
H
5 mV
5 ms
wt/wt
R192Q/R192Q

Figure 8. ACh release parameters and in vivo neuromuscular performance of aged (22-26 months-old) R192Q KI mice. (**A**). Increase (~115%) in MEPP frequency at R192Q diaphragm NMJs (n=5, $p<0.01$). (**B**). Somewhat more pronounced rundown of EPPs at R192Q NMJs during 40 Hz nerve stimulation. (**C**). Effect of extracellular K+ concentration on MEPP frequency at R192Q and wild-type NMJs. At 10 and 15 mM K^+, the MEPP frequency increased disproportionally at R192Q NMJs, but this effect saturated at 30 mM. Example traces of MEPP recordings in different K^+ concentrations are shown at the right-hand side of the panel. (**D**) Quantal content at low rate (0.3Hz) nerve stimulation was equal at R192Q and wild-type NMJs. (**E**) The magnitudes of electrophysiological changes, compared to wild-type, did not different between young and aged R192Q KI mice. (**F**) Effect of selective $Ca_v2.1$ blocker ω-agatoxin-IVA (200 nM) on MEPP frequency and quantal content at NMJs of aged R192Q KI and wild-type mice. (**G**) No change in *in vivo* grip strength test (n=8). (H) RNS-EMG recordings from flexor and lumbricales muscles of the hind foot muscles of anaesthetized R192Q KI and wild-type mice (n=4). Representative traces of 10 consecutive compound muscle action potentials (CMAPs) recorded at 3 Hz stimulation. Traces are superimposed, and then shifted by 1 ms each for easier visualisation. The responses from R192Q and wild-type muscles were similar at all stimulation frequencies tested (0.2 Hz, 1 Hz, 3 Hz, and 5 Hz). Also see Table 2. * $p<0.05$, ** $p<0.01$, *** $p<0.001$.

did not change significantly (Table 2). The average maximum decrement at 3 Hz was 2.9 ± 2.6% and 3.2 ± 2.0% in wild-type and homozygous R192Q KI mice, respectively. This difference was not statistically significant (n=4, p=0.919). Findings at all other frequencies were similar (Table 2). Repetitive CMAPs upon single stimulation, which can occur in the case of increased ACh release at NMJs, were not observed. Fig. 8H shows representative CMAPs recorded in R192Q KI and wild-type mice. Thus, aged R192Q KI mice do not develop muscle weakness.

Table 2. Electromyographical analysis of aged R192Q KI mice

CMAP parameter	Stimulation rate (Hz)	Wild-type	R192Q
Amplitude (mV)	0.2	9.7±2.7	9.8±2.4
	1	9.1±2.8	9.5±2.1
	3	9.0±2.8	9.4±2.3
	5	9.3±2.8	9.3±2.5
Maximal amplitude decrement (%)	0.2	1.9±1.0	0.3±0.9
	1	4.7±2.6	2.0±1.7
	3	2.9±2.6	3.2±2.0
	5	1.5±0.5	3.5±1.5
Maximal area decrement (%)	0.2	2.6±1.2	−3.3±4.9
	1	3.7±2.6	3.0±1.7
	3	1.5±3.5	0.8±3.0
	5	0.3±0.8	1.6±2.5

Repetitive nerve stimulation electromyography recording of compound muscle action potentials (CMAPs) from foot muscles of anaesthetized homozygous R192Q KI and wild-type mice (22 months old) upon supramaximal stimulation of the sciatic nerve. No differences in CMAP amplitude, area or decrement were observed between genotypes. Values are the mean ± S.E.M. of n=4 mice. All p-values were >0.05.

Discussion

We characterized function and morphology of NMJs of R192Q KI mice. The changes in ACh release, most likely due to increased Ca^{2+} influx through the mutated presynaptic $Ca_v2.1$ channels, depended on gene dosage and were present at NMJs of different muscle types throughout the body. The release changes did not result in *in vivo* muscle weakness and were not associated with morphological changes at NMJs. No progressiveness of NMJ changes was observed in aged mice, indicating that the extra presynaptic Ca^{2+} influx, even long-term, was not of such magnitude that apoptotic or necrotic mechanisms were activated.

Gene dosage effect

At heterozygous R192Q KI NMJs, levels of spontaneous ACh release, rundown of 40 Hz evoked release (also see below), and low-rate evoked ACh release at 0.2 mM Ca^{2+} were in-between those measured at wild-types and homozygotes. This indicates a gene dosage effect, which suggests that presynaptic membrane expression of functional R192Q-mutated channels does not differ substantially from wild-type, as shown at R192Q cerebellar granule cell body membranes.[1] Furthermore, it argues against preferred insertion of R192Q-mutated above wild-type channels at active zones.[35] However, at high (10 mM) K^+, spontaneous ACh release was increased to equal levels at hetero- and homozygous NMJs. The reason for this discrepancy at normal versus elevated K^+ remains unclear at present. It may be that Ca^{2+}/calmodulin-dependent channel inactivation[36] is switched on selectively at homozygous terminals at 10 mM K^+, due to a high intracellular Ca^{2+} concentration passing a threshold level. At frog NMJs, high K^+ leads to ACh release at ectopic sites, away from existing active zones.[37] If this were to take place at mouse NMJs, preferential insertion of R192Q-mutated channels at such sites might explain our observation. The finding that high K^+ leads to a disproportional increase in spontaneous transmitter release also at R192Q heterozygous synapses may be of relevance to the human R192Q FHM1 condition, as this follows genetic dominance. Migraine phenomena might therefore be triggered, and promoted, by an exaggerated synaptic response to (temporarily) elevated extracellular K^+ concentration in the brain (also see below).

The increase in spontaneous ACh release at heterozygous R192Q NMJs was completely blocked by ω-agatoxin-IVA, as observed at homozygous NMJs[1], arguing against compensatory involvement of non-$Ca_v2.1$ type channels.

Changes in spontaneous ACh release at R192Q NMJs

NMJ size is positively correlated with spontaneous transmitter release rate.[33,34] However, our fluorescence microscopical measurements demonstrated that the increase in MEPP frequency at R192Q NMJs is not due to synapse growth and thus a direct result of functional changes in R192Q-mutated $Ca_v2.1$ channels.

Increased spontaneous ACh release at R192Q NMJs might reflect a hyperpolarizing shift in the activation voltage of putative low-voltage-activated channels encoded by *Cacna1a*, as proposed earlier by us to be present at NMJs.[38] This is supported by the disproportional increase of MEPP frequency at R192Q NMJs upon K^+ depolarisation. Hyperpolarizing shifts of activation voltages were shown for R192Q-mutated $Ca_v2.1$ channels in transfected cells[39-42] and in cerebellar granule cells of R192Q KI mice.[1]

Experiments with ω-conotoxin-GVIA and ω-agatoxin-IVA, at low extracellular Ca^{2+}, excluded any compensatory involvement of the $Ca_v2.2$ subtype channels and showed complete dependence on $Ca_v2.1$ channels of the increase of spontaneous ACh release at R192Q NMJs.

Increased spontaneous ACh release was also found by us at NMJs of *Tottering* (P601L) and *Rolling Nagoya* (R1262G) mice.[38,43] Moreover, preliminary studies in a new KI mouse with FHM1 mutation S218L also showed a profound increase.[44] Thus, an intriguing synaptic similarity emerges. All these mutations lead to single aminoacid changes at, or near the voltage sensors of segment 4, or the pore-loops between segments 5 and 6 of the transmembrane channel repeats. This hints to a common change in voltage-sensing or its translation into pore opening, causing increased Ca^{2+} flux. However, elevated spontaneous ACh release was also found at NMJs of an EA2 patient with a *truncation* mutation.[14] Functionally, doubling of spontaneous release will not acutely affect impulse transmission at NMJs, since MEPPs do neither affect evoked ACh release nor pass the firing threshold themselves.

Changes in evoked ACh release at R192Q NMJs

At low-rate stimulation (0.3 Hz) in low Ca^{2+} (0.2 mM), we found increased quantal contents in both heterozygous (110 %) and homozygous (245 %) R192Q KI mice. This finding confirms and extends our original observation{van den Maagdenberg, 2004 17 /id}, and indicates increased Ca^{2+} influx through R192Q-mutated presynaptic $Ca_v2.1$ channels. Experiments with ω-conotoxin-GVIA excluded any possible compensatory involvement of the $Ca_v2.2$ subtype channel in the increased evoked ACh release at low Ca^{2+} and, together with the almost complete inhibition of quantal content at homozygous R192Q NMJs by ω-agatoxin-IVA, this indicates that the increase was solely due to

increased Ca^{2+} flux through the R192Q-mutated $Ca_v2.1$ channels. This assumption is further supported by the present finding of increased release probability at R192Q NMJs. The reduced paired-pulse facilitation at low Ca^{2+} can also be explained by larger Ca^{2+} influx at the first pulse at R192Q NMJs, compared to wild-type. The increased size of the readily releasable vesicle pool is also compatible with increased Ca^{2+} influx at R192Q motor nerve terminals, since pool size is dependent on intracellular Ca^{2+} concentration.[45] Increased evoked release due to increased Ca^{2+} flux was predicted from gain-of-function changes in R192Q-mutated single channels in transfected cells.[39,41,42] However, in our previous and present study we did not find an increase at physiological Ca^{2+} concentration (2 mM). Possibly, Ca^{2+} influx under this condition is of such magnitude that presynaptic sensors approached saturation. However, a further increase of ACh release at 5 mM Ca^{2+} argues against complete saturation. Alternatively, Ca^{2+}/calmodulin-dependent channel inactivation[36] might be more active, either due to increased Ca^{2+} influx or as a direct effect of the mutation. The extra rundown of ACh release at R192Q NMJs during the initial phase of high-rate (40 Hz) nerve stimulation, observed at both diaphragm and soleus NMJs, may also result from increased inactivation. However, changed inactivation of R192Q channels was not observed in transfected cells.[39,40] Possibly, such changes only occur in the native, presynaptic environment. The small reduction in high-rate ACh release is not likely to compromise transmission at NMJs, due to a large safety factor at this synapse. This was confirmed by the *in vivo* tests (see below),

No progression of ACh release changes nor development of structural NMJ damage or muscle weakness in aged R192Q KI mice

Long-term increased presynaptic resting Ca^{2+} influx at R192Q NMJs might saturate presynaptic cytosolic Ca^{2+}-buffering systems. The resulting activation of Ca^{2+}-depending signalling pathways or proteases could lead to functional changes, structural damage or even to 'synaptic apoptosis'.[21] Postsynaptically, increased spontaneous ACh release might induce Ca^{2+} overload, like in the slow-channel syndrome, where mutated ACh receptors open for longer periods.[46] However, micro-electrode measurements at diaphragm NMJs of aged (26 months-old) R192Q KI mice did not reveal other or more pronounced electrophysiological differences, compared to wild-types, than observed in the younger groups (3 months-old). The sensitivity of spontaneous and evoked ACh release for $Ca_v2.1$ blocker ω-agatoxin-IVA was also unchanged at aged NMJs, arguing against development of compensatory contribution by other Ca_v channels.

Small motor nerve terminals and increased synaptic vesicles density have been found in muscle biopsy NMJs of *CACNA1A*-mutated EA2 patients.[14] However, NMJs of young and aged R192Q KI mice did not exhibit any morphological abnormalities in

fluorescence- and electron microscopical analyses.

Single-fibre EMG studies on extremities of EA2 patients with known *CACNA1A* mutations, as well as on patients with migraine without proven mutations suggested weakness due to NMJ dysfunction.[14,16] These reports, and our own *ex vivo* finding of extra EPP rundown at 40 Hz stimulation rate at R192Q KI and *Tottering* mouse NMJs[38], prompted us to carry out RNS-EMG studies and muscle strength testing in young and aged R192Q KI mice. However, no CMAP abnormalities or reductions in grip strength were observed. These negative results were not due to technical limitations, because with the same methods we have shown reduced grip-strength and CMAP decrement in studies on the *Rolling Nagoya* mouse (S.Kaja, unpublished data). Furthermore, d-tubocurarine sensitivity in muscle contraction experiments was unchanged, indicating a normal safety factor of neuromuscular transmission. Again, this negative finding could not be explained by technical limitations, because with identical methods we have previously demonstrated increased d-tubocurarine sensitivity in *Tottering* mouse diaphragm *ex vivo*.[38] These findings show that ACh release changes at the R192Q NMJs do not lead to weakness and therefore argue against the hypothesis that muscle weakness is present in human R192Q FHM1. The abnormalities reported for EA2 and migraine with aura were based on single-fiber EMG, which allows for detection of subtle abnormalities ('jitter'). However, single-fiber EMG on FHM1 patients with (I1811L) or without proven *CACNA1A* mutation did not reveal such abnormalities.[20]

The lack of progression in electrophysiological changes and lack of development of morphological damage at NMJs, together with the absence of muscle weakness at young and aged mice, show that increased resting Ca^{2+} influx at R192Q NMJs remains below damaging levels, even in the longer term. It is of interest to note that neurological symptoms in R192Q FHM1 are also non-progressive.

Speculation on R192Q brain synapse function in relation to FHM1 pathogenesis

The findings at R192Q NMJs allow for some speculation on possible changes at FHM1 brain synapses, since $Ca_v2.1$ channels are abundant in brainstem and cortex, areas known to be important in migraine.[47,48] Increased spontaneous release, as present at NMJs, might endanger synaptic transmission by influencing dendritic integration of inhibitory and excitatory evoked responses, which are of low amplitude at brain synapses.[49] Furthermore, the probability of evoked transmitter release is generally low at brain synapses[50], and can in this respect be compared with low-Ca^{2+} conditions at the NMJ. Thus, we predict that those CNS synapses of R192Q KI mice and FHM1 patients that rely mainly on presynaptic $Ca_v2.1$ channels, such as e.g. cerebellar Purkinje cells, have increased evoked transmitter output. At many other synapses the situation may, however,

be complicated by the interchangeable, joint contribution of $Ca_v2.1$, $Ca_v2.2$ (N-type) and $Ca_v2.3$ (R-type) channels in transmitter release. Recently, reduced fractional contribution by $Ca_v2.1$ channels to glutamate release was observed in cultured hippocampal neurons transfected with R192Q and other FHM1 mutant channels, while overall release remained constant.[35]

Glutamate release in cortical synapses is important for CSD and is controlled by $Ca_v2.1$ channels.[51] Thus, increased glutamate release, and disproportional effects thereupon by either high extracellular K^+ or low Ca^{2+} concentration, which may evolve during CSD[52], might underlie CSD susceptibility of R192Q KI mice.[1]

Acknowledgements

The authors thank Mr. P. van Someren for technical assistance, Mr. H.T. van der Leest for help with Matlab programming, Dr. H. Putter for statistical advice and Dr. C.L. Thompson (University of Durham, UK) and professor J.H.J. Wokke (UMC Utrecht) for helpful discussions. The Department of Cell Biology at the UMC Utrecht provided excellent electron microscopical service. Dr. J.N. Noordermeer (Dept. of Molecular Cell Biology) kindly allowed the use of the fluorescence microscope. This work was supported by grants from the Prinses Beatrix Fonds (#MAR01-0105, to JP), the Hersenstichting Nederland (#9F01(2).24, to JP), KNAW van Leersumfonds (to JP), the Netherlands Organisation for Scientific Research, NWO (an EMBL travel bursary to SK, and a VICI grant 918.56.602, to MDF), a 6th Framework specific targeted research project EUROHEAD (LSHM-CT-2004-504837, to MDF) and the Center for Medical Systems Biology (CMSB) established by the Netherlands Genomics Initiative/Netherlands Organisation for Scientific Research (NGI/NWO).

References

1. van den Maagdenberg,A.M. et al. A Cacna1a knockin migraine mouse model with increased susceptibility to cortical spreading depression. Neuron 41, 701-710 (2004).
2. Wheeler,D.B., Randall,A., Sather,W.A. & Tsien,R.W. Neuronal calcium channels encoded by the alpha 1A subunit and their contribution to excitatory synaptic transmission in the CNS. *Prog. Brain Res.* **105**, 65-78 (1995).
3. Uchitel,O.D. *et al.* P-type voltage-dependent calcium channel mediates presynaptic calcium influx and transmitter release in mammalian synapses. *Proc. Natl. Acad. Sci. U. S. A* **89**, 3330-3333 (1992).
4. Mori,Y. *et al.* Primary structure and functional expression from complementary DNA of a brain calcium channel. *Nature* **350**, 398-402 (1991).
5. Stea,A. *et al.* Localization and functional properties of a rat brain alpha 1A calcium channel reflect similarities to neuronal Q- and P-type channels. *Proc. Natl. Acad. Sci. U. S. A* **91**, 10576-10580 (1994).
6. Bourinet,E. *et al.* Splicing of alpha 1A subunit gene generates phenotypic variants of P- and Q-type calcium channels. *Nat. Neurosci.* **2**, 407-415 (1999).
7. Imbrici,P. *et al.* Dysfunction of the brain calcium channel CaV2.1 in absence epilepsy and episodic ataxia. *Brain* **127**, 2682-2692 (2004).
8. Jouvenceau,A. *et al.* Human epilepsy associated with dysfunction of the brain P/Q-type calcium channel. *Lancet* **358**, 801-807 (2001).
9. Ophoff,R.A. *et al.* Familial hemiplegic migraine and episodic ataxia type-2 are caused by mutations in the Ca2+ channel gene CACNL1A4. *Cell* **87**, 543-552 (1996).
10. Zhuchenko,O. *et al.* Autosomal dominant cerebellar ataxia (SCA6) associated with small polyglutamine expansions in the alpha 1A-voltage-dependent calcium channel. *Nat. Genet.* **15**, 62-69 (1997).
11. Felix,R. Insights from mouse models of absence epilepsy into Ca2+ channel physiology and disease etiology. *Cell Mol. Neurobiol.* **22**, 103-120 (2002).
12. Plomp,J.J., van den Maagdenberg,A.M., Molenaar,P.C., Frants,R.R. & Ferrari,M.D. Mutant P/Q-type calcium channel electrophysiology and migraine. *Curr. Opin. Investig. Drugs* **2**, 1250-1260 (2001).
13. Kim,Y.I. & Neher,E. IgG from patients with Lambert-Eaton syndrome blocks voltage-dependent calcium channels. *Science* **239**, 405-408 (1988).
14. Maselli,R.A. *et al.* Presynaptic failure of neuromuscular transmission and synaptic remodeling in EA2. *Neurology* **61**, 1743-1748 (2003).
15. Jen,J. *et al.* Loss-of-function EA2 mutations are associated with impaired neuromuscular transmission. *Neurology* **57**, 1843-1848 (2001).
16. Ambrosini,A., Maertens,d.N. & Schoenen,J. Neuromuscular transmission in migraine: a single-fiber EMG study in clinical subgroups. *Neurology* **56**, 1038-1043 (2001).
17. Ambrosini,A., Pierelli,F. & Schoenen,J. Acetazolamide acts on neuromuscular transmission abnormalities found in some migraineurs. *Cephalalgia* **23**, 75-78 (2003).
18. Jen,J. *et al.* Loss-of-function EA2 mutations are associated with impaired neuromuscular transmission. *Neurology* **57**, 1843-1848 (2001).
19. Schelhaas,H.J., Van de Warrenburg,B.P., Kremer,H.P. & Zwarts,M.J. Neuromuscular transmission in SCA6. *Ann. Neurol.* **55**, 451-452 (2004).
20. Terwindt,G.M., Kors,E.E., Vein,A.A., Ferrari,M.D. & van Dijk,J.G. Single-fiber EMG in familial hemiplegic migraine. *Neurology* **63**, 1942-1943 (2004).
21. Mattson,M.P., Keller,J.N. & Begley,J.G. Evidence for synaptic apoptosis. *Exp. Neurol.* **153**, 35-48 (1998).
22. Lakso,M. *et al.* Efficient in vivo manipulation of mouse genomic sequences at the zygote stage. *Proc. Natl. Acad. Sci. U. S. A* **93**, 5860-5865 (1996).
23. Plomp,J.J., van Kempen,G.T. & Molenaar,P.C. Adaptation of quantal content to decreased postsynaptic sensitivity at single endplates in alpha-bungarotoxin-treated rats. *J Physiol* **458**, 487-499 (1992).
24. Magleby,K.L. & Stevens,C.F. A quantitative description of end-plate currents. *J Physiol* **223**, 173-197 (1972).

25. McLachlan,E.M. & Martin,A.R. Non-linear summation of end-plate potentials in the frog and mouse. *J Physiol* **311**, 307-324 (1981).
26. Miyamoto,M.D. Binomial analysis of quantal transmitter release at glycerol treated frog neuromuscular junctions. *J Physiol* **250**, 121-142 (1975).
27. Stevens,C.F. & Tsujimoto,T. Estimates for the pool size of releasable quanta at a single central synapse and for the time required to refill the pool. *Proc. Natl. Acad. Sci. U. S. A* **92**, 846-849 (1995).
28. Luft,J.H. Improvements in epoxy resin embedding methods. *J Biophys. Biochem. Cytol.* **9**, 409-414 (1961).
29. Reynolds,E.S. The use of lead citrate at high pH as an electron-opaque stain in electron microscopy. *J Cell Biol.* **17**, 208-212 (1963).
30. Tilson,H.A. & Cabe,P.A. Assessment of chemically-induced changes in the neuromuscular function of rats using a new recording grip meter. *Life Sci.* **23**, 1365-1370 (1978).
31. Bewick,G.S. Maintenance of transmitter release from neuromuscular junctions with different patterns of usage “in vivo”. *J Neurocytol.* **32**, 473-487 (2003).
32. Schneggenburger,R. & Neher,E. Intracellular calcium dependence of transmitter release rates at a fast central synapse. *Nature* **406**, 889-893 (2000).
33. Harris,J.B. & Ribchester,R.R. The relationship between end-plate size and transmitter release in normal and dystrophic muscles of the mouse. *J Physiol* **296**, 245-265 (1979).
34. Kuno,M., Turkanis,S.A. & Weakly,J.N. Correlation between nerve terminal size and transmitter release at the neuromuscular junction of the frog. *J Physiol* **213**, 545-556 (1971).
35. Cao,Y.Q. *et al.* Presynaptic Ca2+ channels compete for channel type-preferring slots in altered neurotransmission arising from Ca2+ channelopathy. *Neuron* **43**, 387-400 (2004).
36. Lee,A. *et al.* Ca2+/calmodulin binds to and modulates P/Q-type calcium channels. *Nature* **399**, 155-159 (1999).
37. Ceccarelli,B., Fesce,R., Grohovaz,F. & Haimann,C. The effect of potassium on exocytosis of transmitter at the frog neuromuscular junction. *J Physiol* **401**, 163-183 (1988).
38. Plomp,J.J. *et al.* Abnormal transmitter release at neuromuscular junctions of mice carrying the tottering alpha(1A) Ca(2+) channel mutation. *Brain* **123 Pt 3**, 463-471 (2000).
39. Hans,M. *et al.* Functional consequences of mutations in the human alpha1A calcium channel subunit linked to familial hemiplegic migraine. *J. Neurosci.* **19**, 1610-1619 (1999).
40. Kraus,R.L., Sinnegger,M.J., Glossmann,H., Hering,S. & Striessnig,J. Familial hemiplegic migraine mutations change alpha1A Ca2+ channel kinetics. *J Biol. Chem.* **273**, 5586-5590 (1998).
41. Kraus,R.L. *et al.* Three new familial hemiplegic migraine mutants affect P/Q-type Ca(2+) channel kinetics. *J Biol. Chem.* **275**, 9239-9243 (2000).
42. Tottene,A. *et al.* Familial hemiplegic migraine mutations increase Ca(2+) influx through single human CaV2.1 channels and decrease maximal CaV2.1 current density in neurons. *Proc. Natl. Acad. Sci. U. S. A* **99**, 13284-13289 (2002).
43. Plomp,J.J., van den Maagdenberg,A.M., Ferrari,M.D., Frants,R.R. & Molenaar,P.C. Transmitter release deficits at the neuromuscular synapse of mice with mutations in the Cav2.1 (alpha1A) subunit of the P/Q-type Ca2+ channel. *Ann. N. Y. Acad. Sci.* **998**, 29-32 (2003).
44. Kaja,S. *et al.* Increased transmitter release at neuromuscular synapses of a novel Cacna1a S218L knock-in mouse model for familial hemiplegic migraine. *Society for Neuroscience Annual Meeting Abstract* (2004).
45. Smith,C., Moser,T., Xu,T. & Neher,E. Cytosolic Ca2+ acts by two separate pathways to modulate the supply of release-competent vesicles in chromaffin cells. *Neuron* **20**, 1243-1253 (1998).
46. Vohra,B.P. *et al.* Focal caspase activation underlies the endplate myopathy in slow-channel syndrome. *Ann. Neurol.* **55**, 347-352 (2004).
47. Goadsby,P.J., Lipton,R.B. & Ferrari,M.D. Migraine--current understanding and treatment. *N. Engl. J Med.* **346**, 257-270 (2002).
48. Pietrobon,D. & Striessnig,J. Neurobiology of migraine. *Nat. Rev. Neurosci.* **4**, 386-398 (2003).
49. Stevens,C.F. Quantal release of neurotransmitter and long-term potentiation. *Cell* **72 Suppl**, 55-63 (1993).

50. Hessler,N.A., Shirke,A.M. & Malinow,R. The probability of transmitter release at a mammalian central synapse. *Nature* **366**, 569-572 (1993).

51. Turner,T.J., Adams,M.E. & Dunlap,K. Calcium channels coupled to glutamate release identified by omega-Aga-IVA. *Science* **258**, 310-313 (1992).

52. Somjen,G.G. Mechanisms of spreading depression and hypoxic spreading depression-like depolarization. *Physiol Rev.* **81**, 1065-1096 (2001).